JOURNAL OF MATERIALS SCIENCE **34** (1999) 783–794

Computer simulation of grain growth by grain boundary migration during liquid phase sintering

Z. S. NIKOLIC
University of Nish, Faculty of Electronic Engineering, Department of Microelectronics, 18000 Nish, P.O. Box 73, Yugoslavia
E-mail: zhikolic@elfak.ni.ac.yu

From many experiments with mixtures of small and large particles, it can be concluded that during liquid phase sintering, smaller particles partially dissolve and a solid phase precipitates on the larger particles. Therefore, the number of smaller particles decreases due to coarsening. The growth rate can be controlled either by the solid-liquid phase boundary reaction or by diffusion through the liquid phase. This dissolution-reprecipitation process leads to further densification by rearrangement of smaller and larger particles. The microstructure may change either by larger particles growing during the Ostwald ripening process or by shape accommodation. In this study, two-dimensional simulation of grain growth by grain boundary migration based on such a physical and corresponding numerical modeling of liquid phase sintering was considered. The simulation method developed is based on the defined submodels for model system definition, for solution-precipitation, and for grain coarsening process.

1. Introduction

Numerous researchers have studied liquid phase sintering during the past few decades, beginning with Lenel [1]. In particular, there are a large number of theoretical and experimental studies of grain growth. Liquid phase sintering is an important process for the production of many ceramic materials. One important aspect of its application is that it enhances densification and affects microstructural development. The main characteristic of this process is that the composition of the powder and the firing temperature must be chosen such that a small amount of liquid forms between the grains. Accordingly, the powder compact must satisfy three general requirements: (1) there is a liquid phase at the sintering temperature, (2) the solid phase is soluble in the liquid, and (3) the liquid wets the solid. This process is especially important for systems that are difficult to densify by solid state sintering or when the use of solid state sintering requires high sintering temperatures. Unfortunately, the liquid phase used to promote sintering in most cases remains as a glassy grain boundary phase that may lead to a deterioration of materials' properties.

A particularly interesting approach which leads better understanding of liquid phase sintering phenomena is the application of numerical procedures, because they have great flexibility and can be used to obtain solutions for any model system configuration. In recent years, a range of computer simulation models have been developed with the aim of simulating the detailed evolution of microstructure during grain growth. Recently the results of a computer simulation of boundary migration during liquid phase sintering have been reported [2]. This paper describes the computer-based simulation method that has been developed for determination of a qualitative and a quantitative effect of a moving grain boundary on the solid/liquid interface during liquid phase sintering. The grain boundary migration means that solid atoms that are dissolved on one side of the boundary transport across the liquid layer and deposit on the other side of the boundary.

2. Process modeling

Generally speaking, the liquid phase sintering is viewed in terms of three overlapping stages: particle rearrangement, solution-precipitation, and Ostwald ripening. However, each stage is identified by the dominant mechanism occurring in that stage. Our theoretical analysis assumes a numerical definition of submodels for initial model system definition, solution-precipitation process, and grain coarsening process and their successive realization during process simulation. Note that these processes are not modeled as sequential events.

First, there must be a mixture of two powders: a major component that forms the particulate solid, and an additive phase as a liquid-producing component. It is assumed that the liquid wets and spreads to cover the solid particle surfaces, so that they will be separated by a liquid layer.

A model system of N contours (closed boundaries as two-dimensional (2-D) particle representation) of solid phase in the liquid represented by spherical particles

within the smallest enclosing square box, and not allowing the particles to lie outside the square box (rectangular domain area × the largest contour's diameter) is assumed. This model will be based on the assumption that there are no pores during liquid phase sintering. In order to model the system with a large amount of liquid, the center-to-center approach within a distance ℓ (the minimal thickness of the liquid layer) is not allowed (i.e., contour–contour interactions are removed).

The model system contours can be represented as an array of moving points, using the boundary points of contours (sites located on the contour boundary or on the phase interface):

$$D^s = \left\{\mathbf{R}^s; \mathbf{r}_1^s, \mathbf{r}_2^s, \ldots, \mathbf{r}_{n_s}^s\right\} \quad (s = 1, 2, \ldots, N)$$

where $\mathbf{R}^s$ is the position vector of the center of the s-th contour, and $\mathbf{r}_l^s$ is the position vector of the l-th point on the interface of this contour with its origin at the center of the contour, and n_s is the number of its boundary points. Then the union

$$\bigcup_{s=1}^{N} D^s$$

is the solid phase within the model system. A time-dependent microstructure will be mapped onto a 2-D by three discrete matrixes: the integer matrix $\|e_{ij}\|_{n\times m}$, where the value of the element e_{ij} indicates the phase present at the point (i, j), so that

$$e_{ij} = \begin{cases} 0 & \text{for liquid phase} \\ >0 & \text{for solid phase, i.e. } 1, 2, \ldots, N \end{cases}$$

and two real matrixes for the concentration $\|c_{ij}\|_{n\times m}$ and the flux $\|f_{ij}\|_{n\times m}$. Thus, its domain and the topological information concerning contour neighbors characterize each contour.

If

$$S_o = \{(\mathbf{R}^s, \mathbf{r}^s) \,|\, (\mathbf{R}^s, \mathbf{r}^s) \in D_o^s, \quad s = 1, 2, \ldots, N\}$$

is the initial structure of the model system, and

$$S_t = \{(\mathbf{R}^s, \mathbf{r}^s) \,|\, (\mathbf{R}^s, \mathbf{r}^s) \in D_t^s, \quad s = 1, 2, \ldots, N\}$$

is the structure of contours after sintering (simulation) time t, then the transformation $S_o \rightarrow S_t$ describes the liquid phase sintering of the model system.

2.1. Initial model system

The starting model system is characterized by a contour size distribution that is generated by random generation (the standard normal distribution function) for given contour size region $[r_{\min}, r_{\max}]$. In this generation, all radii generated out of defined size region will be ignored. The center positions of the contours are randomly distributed ("gravity free" and "drop-freeze" methodology) without contour intersection and excluding all those that are within any previously packed contours (Fig. 1a). Notice that for this random generating procedure, one can used any specified size distribution.

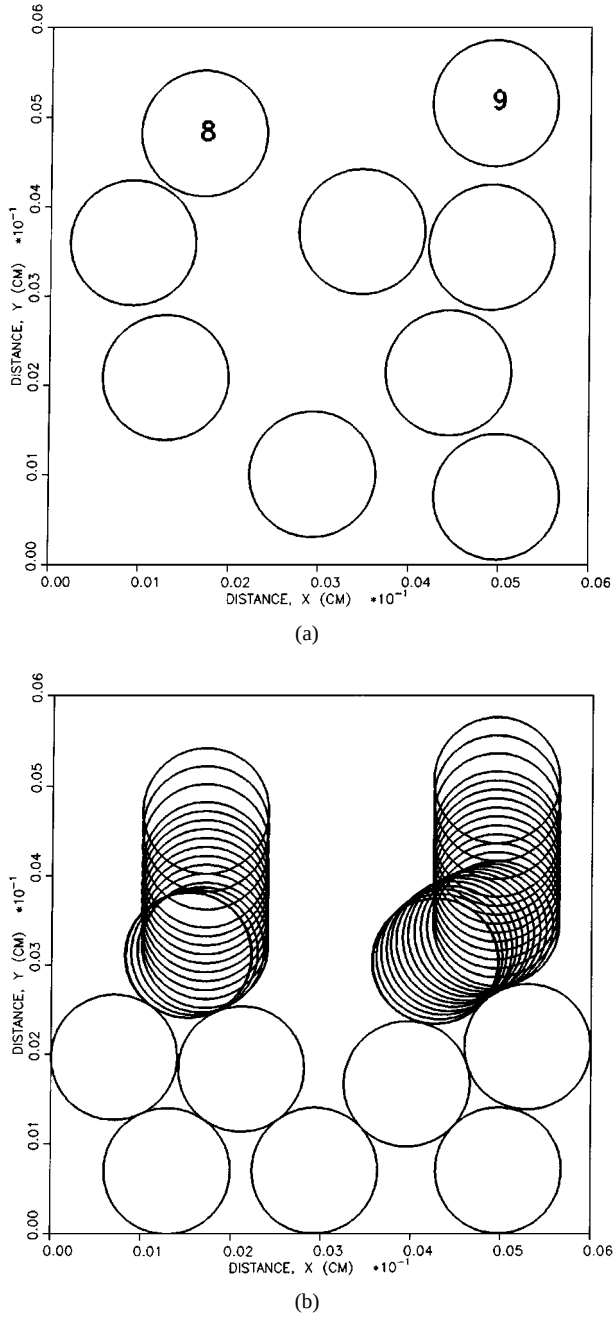

(a)

(b)

Figure 1 Simulation of packing process: (a) initial monosized contour distribution generated by random generator, (b) packed model system with displayed steps of packing contours numbered with **8** and **9**.

The influence of particle shape on packing efficiency has been recognized for a long time. However, most of the studies deal with the packing of spherical or nearly spherical particles, whereas the studies of packing of nonspherical particle mixture appear to be limited.

The packing process assumes that if there is good wetting between liquid and solid phase, solid particles will rearrange themselves under the action of surface tension forces, producing a more stable packing. The method applied for the simulation of the initial packing process (PP0) is the settling procedure in which contours are subjected to a simulated gravity field: the

contour falls under gravity and slides down over the already settled contours. This procedure will be applied to each contour starting with the contour having the lowest position in the vertical direction of experimental region (Fig. 1b). To avoid wall effects, this procedure was applied so that packed domains were within an interior region that has its boundary at least a few ℓ (1 to 2) inside the outer boundary wall of experimental region.

It is assumed that the bottom wall and walls on both sides of the experimental region are stationary and that the upper wall is the moving wall. Now a new (final) experimental region in which the upper wall position is defined by the highest contour position can be defined.

The number and the sizes of contours and its center positions characterize the initial model structure. The key parameters, such as contact and dihedral angle, amount of liquid phase, the minimal thickness of the liquid layer, and distribution of the liquid phase between the solid grains are all directly defined by or calculated from the model system structure.

2.2. Solution-precipitation process

The main characteristic of the solution-precipitation process is that the smaller solid grains dissolve at solid/liquid interface (thermodynamically unstable), diffuse through the liquid, and precipitate on the larger grains.

A system consisting of a dispersion of spherical particles with different radii in a liquid (Fig. 2a) in which the solid phase has some solubility is assumed. Thus, the concentration of the dissolved solid, C, around a particle of radius r is given by the Gibbs-Thomson equation

$$\ln\left(\frac{C}{C_o}\right) = \frac{2\gamma_{sl}\Omega}{kT} \cdot \frac{1}{r} \tag{1}$$

where C_o is the equilibrium concentration of liquid in contact with the flat solid, γ_{sl} is the solid/liquid interfacial energy, Ω is the molecular volume of the solid, and kT has its usual meaning. If $\Delta C = C - C_o$ is small, then Equation 1 becomes

$$\Delta C = C_o \cdot \frac{2\gamma_{sl}\Omega}{kT} \cdot \frac{1}{r} \tag{2}$$

This equation is not valid for a very small particle because ΔC becomes infinite as its radius goes to zero. However, the number of the small particles at any simulation time is sufficiently small so that Equation 2 can be assumed to be valid for all particles.

Notice that after simulation time $t > 0$, most of the particles are no longer circular because the diffusion field around and between particles becomes highly asymmetric.

It can be seen from Equation 2 that the concentration at an interface with high curvature will be above that at an interface with low curvature, thus a higher concentration around a smaller particle gives rise to a net flux of matter from the smaller to the larger one (Fig. 2b). If D_L is the concentration independent diffusivity of the solid in the liquid, then the flux vector is

$$\mathbf{J} = -D_L \nabla C \tag{3}$$

Applying Equation 3 at boundary points of solid interface, the effects of the dissolution and precipitation processes can be computed.

This process is accompanied by considerable coarsening and by changes in the shape of particles. The sizes of the particles and their locations change as simulation time increases: smaller particles dissolve, and the dissolving material deposits on the large particles in such a way that grain shape accommodation occurs. Thus, the particles can pack more efficiently because of a nonspherical–symmetric diffusion field. The space left by the small dissolved particles is recovered by packing process. This process (PP1) is also modeled by the settling procedure in which contours settle toward the center of experimental region. This procedure can be described by contour motion

$$D^s \rightarrow D'^s,$$

where D'^s is the domain position of s-th contour after partially settling. The new domain must be restricted to those regions not already occupied by other domains, for example,

$$D'^s \cap D^j = \emptyset (j = 1, 2, \ldots, N; s \neq j).$$

Such settling process brings all contours close one to another with the contour distance not less than the minimal thickness of liquid layer, ℓ.

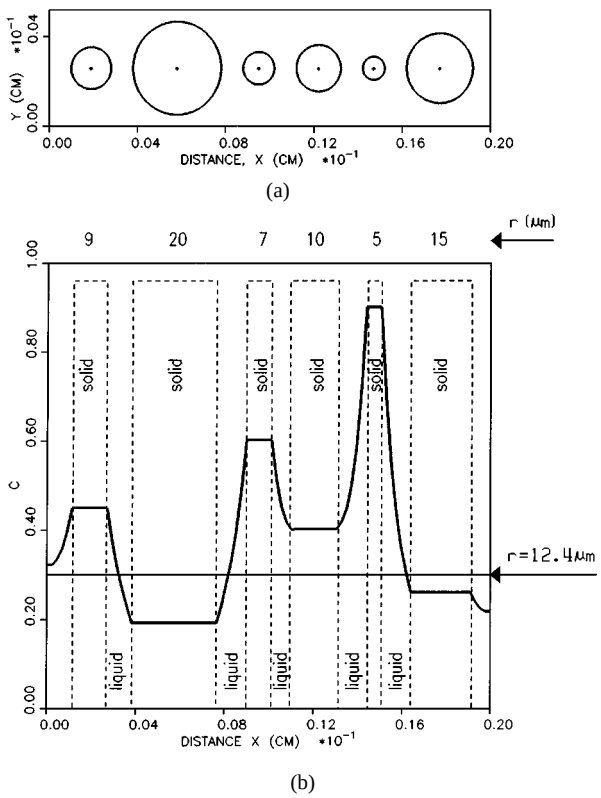

Figure 2 Contour coarsening modeling: (a) model system of six contours of different radii, (b) corresponding (normalized) concentration profile of liquid along the x-axis (solid line). The horizontal line marks critical concentration of liquid that corresponds to the critical particle size r^*.

The initial liquid concentration can be taken as the concentration of pure liquid with no dissolved solid. However, because the dissolution process starts very quickly after the additive melts, the same results can be obtained with equilibrium liquid concentration or with minimal liquid/solid interface concentration as the initial concentration [3]. The model assumes that the liquid phase is uniformly distributed into a model system.

The boundary composition is not constant during simulation. It changes with time as a function of diffusion in the liquid and of amount of dissolved solid phase [4]: boundary concentration can increase or decrease but the material's flow outside the experimental region is not allowed. Time dependent boundary concentration is especially important for a particle that is located near the edge of the experimental region to avoid the effects of finite model system size. When the amount of liquid is relatively small and is located in the contact region only between the solid particles, the boundary concentration can be defined as given in [5].

2.3. Contour coarsening

If the solid particles are dispersed in the liquid phase, the grain coarsening is called Ostwald ripening process. If the solid phase forms a dense polyhedral grain structure, grain growth is due by grain boundary migration that is characterized by dissolution of smaller grains in the liquid, by its transportation through the liquid, and by precipitation on the larger ones.

Grain coarsening is a typical multibody free boundary problem in which the domains alter their morphologies in response to the diffusion field. After solution-precipitation, the particles grow in supersaturated liquid phase, and after the supersaturation becomes small, large particles start to grow at the expense of small particles. This tendency for particles to grow or to shrink depends on the size of particles relative to a critical particle size (zero-growth, i.e., the radius of critical particle for which $dr/dt = 0$), r^* [6]. For reaction controlled growth $r^* = 9\langle r\rangle/8$, and for diffusion controlled growth, $r^* = \langle r\rangle$, where $\langle r\rangle$ is the arithmetic mean particle size.

In that sense, the theoretical basis for modeling of this process is the assumption that at any given moment the contours smaller than a critical contour size will dissolve, surrounding themselves with a zone of excess solute that will migrate to the contours larger than r^*, and these therefore grow. Notice that the critical contour size is time-dependent, i.e., $r^*(t)$. For the system shown in Fig. 2a, assumed reaction controlled growth $r^* = 12.4$ μm, dissolved material from four smallest contours precipitates on the two largest contours (Fig. 2b) during contour coarsening process.

This simulation method assumes that the liquid volume change depends on solution and precipitation processes. After cooling, liquid forms a glassy grain boundary phase with no solid solution, no crystallization, and no evaporation. A similar sintering process generally characterizes most of the systems.

3. Process simulation

Mass diffusion outside the particles is assumed to be the only mass transfer process. Diffusion through the liquid phase is defined by the partial differential equation of the parabolic type

$$\frac{\partial C}{\partial t} = D_L \cdot \nabla^2 C \tag{4}$$

If $C = C(x, y, t)$, Equation 4 can be replaced by

$$\frac{\partial C}{\partial t} = D_L \cdot \left(\frac{\partial^2 C}{\partial x^2} + \frac{\partial^2 C}{\partial y^2}\right) \tag{5}$$

For the computation of time-dependent concentration of liquid phase (the numerical solution of Equation 5) finite-difference technique will be used.

An experimental domain of a rectangular shape that is partitioned into subregions by a mesh is assumed. There are the two distance coordinates x and y, and time t as independent variables, and that the respective grid spacings are Δx, Δy, and Δt. Subscripts i, j, and k may then be used to denote that space point having coordinates $i\,\Delta x$, $j\,\Delta y$, and $k\,\Delta t$, so called the grid-point (i, j, k). For an approximate solution of the Equation 5, the classical five points approximation (the Schmidt method) can be used [7]

$$\begin{aligned} c_{i,j,k+1} = {} & (1 - 2\lambda_1 - 2\lambda_2)c_{i,j,k} \\ & + \lambda_1(c_{i+1,j,k} + c_{i-1,j,k}) \\ & + \lambda_2(c_{i,j+1,k} + c_{i,j-1,k}) \\ & (i = 2, 3, \ldots, n-1;\ j = 2, 3, \ldots, m-1; \\ & k = 0, 1, \ldots) \end{aligned} \tag{6}$$

where $\lambda_1 = D_L\,\Delta t/(\Delta x)^2$, and $\lambda_1 = D_L\,\Delta t/(\Delta y)^2$. If all the $c_{i,j,k}$ at the time level t_k are known, $c_{i,j,k+1}$ at the time level t_{k+1} can be calculated for all i and j directly using Equation 6. For reasons of computational stability, values of distance and time interval (Δx, Δy, and Δt) must also be taken so that $\lambda_1 + \lambda_2$ does not exceed 0.5. The defined model assumes the contours' surfaces that have discretized with equal-sized squares. The same discretization was used for approximating the curvature at the contour's surface.

With the above mentioned facts as the starting assumption, the simulation method (the defined computer procedure) will be as follows:

A Definition of model system for the given experimental region, for N, $[r_{\min}, r_{\max}]$ and ℓ.

If (x_c^s, y_c^s) and r_s are the center position and the initial radius of the s-th contour, respectively, then the solid phase of the model system is

$$\bigcup_{s=1}^{N} \left\{(x_i, y_j) \middle| \left(x_i - x_c^s\right)^2 + \left(y_j - y_c^s\right)^2 \le r_s^2\right\}$$

with the contours' boundary points

$$D^s = \left\{(x_i, y_j) \,\middle|\, \left(x_i - x_c^s\right)^2 + \left(y_j - y_c^s\right)^2 = r_s^2\right\}$$
$$(s = 1, 2, \ldots, N)$$

After packing procedure PP0, all contours of the initial model structure will be numbered and recorded.

B Process simulation

B.1 Computation of the diffusion field around the model system contours, i.e. computation of $c_{i,j,k+1}$ from $c_{i,j,k}$ in all points of liquid, by applying Equation 6

After simulation time $t > 0$, most of the contours will no longer be circular because the diffusion field around and between contours is highly asymmetric. For 2-D simulation and for the very short simulation time, one can assume that the contours are approximately circular, thus the radius of s-th contour can be computed by

$$r_s = \sqrt{A^s/\pi},$$

where A^s is the area of the contour. For this case, the contour's area can be directly obtained by summing the number of mesh points within the contour. However, because each contour is a closed polygon approximated by n_s line segments, the area within a 2-D curve enclosed by n_s line segments is [8]

$$A^s = \frac{1}{2}\left\{\left(x_1^s y_2^s + x_2^s y_3^s + \cdots + x_{n_s-1}^s y_{n_s}^s + x_{n_s}^s y_1^s\right)\right.$$
$$\left. - \left(x_2^s y_1^s + x_3^s y_2^s + \cdots + x_{n_s}^s y_{n_s-1}^s + x_1^s y_{n_s}^s\right)\right\}$$
$$(s = 1, 2, \ldots, N) \quad (7)$$

For a long simulation time and for the Gibbs-Thomson boundary condition for the solid-liquid interface of the form

$$C\left(\mathbf{r}_j^s\right) \sim \kappa\left(\mathbf{r}_j^s\right) \quad \text{for} \quad \mathbf{r}_j^s \quad \text{on} \quad D^s \qquad (8)$$

where $\kappa(\mathbf{r}_j^s)$ is the curvature at $\mathbf{r}_j^s$, the most important numerical consideration in performing an accurate computation is the determination of the curvature of noncircular contour. In this sense, the better way would be to calculate the local curvature numerically, for example, using the interpolation functions at each boundary point separately. If one needs a smooth function for describing the contour-boundaries, then a cubic polynomial could be the simplest function of this type, as recognized by Saetre and Ryum [9] and applied by Cocks and Gill [10]. In this simulation method the curvature at each point on domain D^s was computed by fitting a quadratic polynomial to the point and its two neighbors. Notice that for a square mesh, a sharp curvature on contour-boundary requires a very fine mesh.

B.2 Computation of the flux at the boundary points D^s $(s = 1, 2, \ldots, N)$

The flux through the finite element $(\Delta x \times \Delta y)$ of solid phase boundary point (x_i, y_j) is

$$J_{i,j} = J_{i,j}^x + J_{i,j}^y, \qquad (9)$$

where Equation 9 is two-dimensional case of Equation 3. Because the process model is based on the assumption that solution, diffusion, and precipitation processes take place in the liquid phase and that solid–solid interactions are not allowed, then

$$J_{i,j}^x = -D_L \cdot \left(\frac{c_{i,j} - c_{i+1,j}}{\Delta x} \cdot \delta_{i+1,j} + \frac{c_{i,j} - c_{i-1,j}}{\Delta x} \cdot \delta_{i-1,j}\right)$$

$$J_{i,j}^y = -D_L \cdot \left(\frac{c_{i,j} - c_{i,j+1}}{\Delta y} \cdot \delta_{i,j+1} + \frac{c_{i,j} - c_{i,j-1}}{\Delta y} \cdot \delta_{i,j-1}\right)$$

where

$$\delta_{i,j} = \begin{cases} 1 & \text{if } (i, j) \in \text{ liquid phase} \\ 0 & \text{if } (i, j) \in \text{ solid phase} \end{cases}$$

B.3 Computation of mass flow, dM/dt, in all boundary points of solid phase

B.4 Determination of a new topology of the model system: the evolution of the centers of mass as a reference point for model system contours and the domains' position, i.e.

$$D^s = \left\{\mathbf{R}^s(t); \mathbf{r}_1^s(t), \mathbf{r}_2^s(t), \ldots, \mathbf{r}_{n_s}^s(t)\right\}$$
$$(s = 1, 2, \ldots, N).$$

During the simulation process the simulator continuously checks for possible new contours' position and new geometry. All topological information is recorded and saved for each time interval for the next analysis and computation.

The domains $D^s(t)$ are stored and each successive new domains' position calculated as a function of time, i.e., the domains' definition updated by

$$D^s(t + \Delta t) = D^s(t) + \Delta D^s(\Delta t) \;\; (s = 1, 2, \ldots, N)$$

where new subdomain (domains' increment) $\Delta D^s(\Delta t)$ is a result of current dissolution effects ($dM/dt < 0$ or a negative growth rate, $dA^s/dt < 0$) and/or precipitation effects ($dM/dt > 0$ or a positive growth rate, $dA^s/dt > 0$), as well as new domains' locations because contours will rearrange themselves under the action of surface tension forces producing a more stable packing (PP1). As shown in Fig. 3, where $\mathbf{n}_{i,j}$ is the

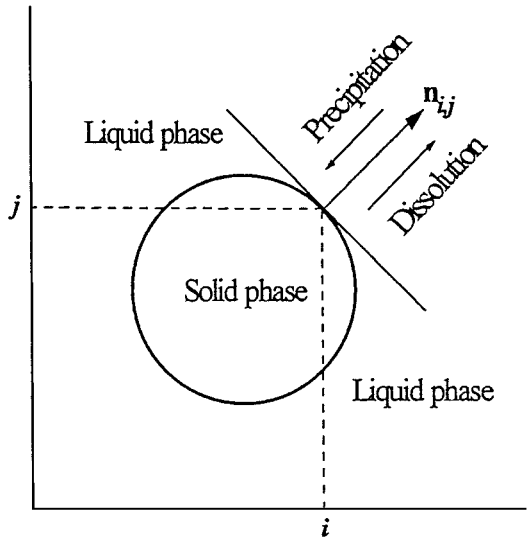

Figure 3 Schematic diagram illustrating solution-precipitation process direction.

normal vector to the contour, the dissolution is directed from the contour toward the liquid phase, and the precipitation toward the contour. For the latter, each new boundary point would be located with respect to the old boundary point and corresponding line segments. A suitable direction for the definition of the new point could be determined either by concentration gradient or by random generation. Because a new point's positions are very close to the old ones, they would be defined in an approximately radial direction.

From time to time it is required to make the elementary topological transformation: as a result of the dissolution process a contour smaller than the finite element of mesh ($\Delta x \times \Delta y$, i.e. four boundary points) will be remove from the system. The very small contours disappear by giving their mass to surrounding contours. Because the times required to diffuse these contours into the liquid are very small compared with the time interval Δt, it is expected that the change of the diffusion field of the surrounding contours during the simulation time Δt is not greatly affected by the removed contours.

This procedure has been developed for a 2-D model system, but can be easily extended to include a third dimension. The fact is, however, that the topological changes that occur in 3-D are more complex than those that occur in 2-D.

4. Results and discussion

The present simulation method and the computer program itself were tested in order to conduct a study of grain boundary migration during liquid phase sintering of an Al_2O_3-glass system. Such a system is relatively well characterized. The observation that the alumina–glass system has a continuous glassy boundary [11–13] indicates good wetting. Hence, it can be used as a model system.

An initial model system (Fig. 4a) was obtained by applying random generating methodology and assuming

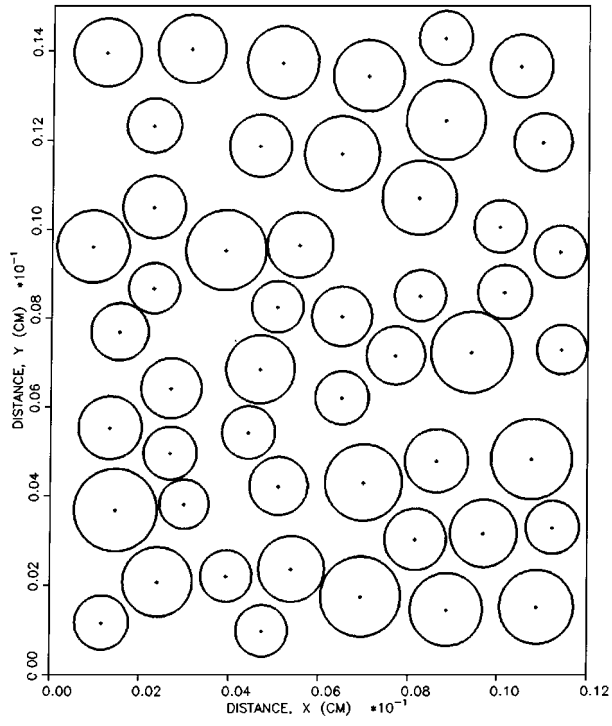

(a)

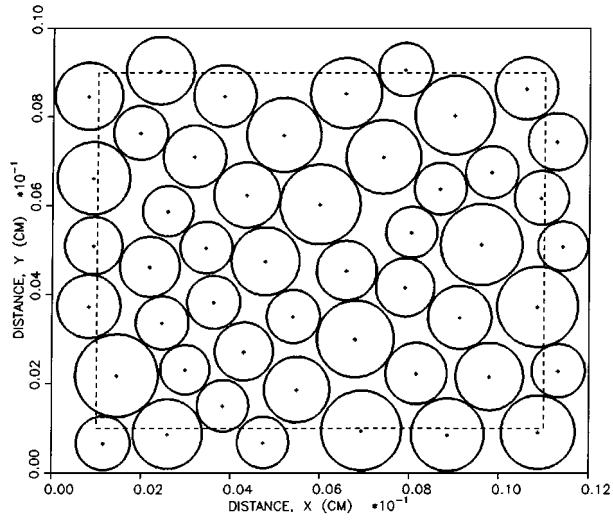

(b)

Figure 4 Geometry of investigated model system for Al_2O_3—glass system: (a) before packing, (b) after packing.

that for the polycrystalline Al_2O_3, the particle size range was 5–10 μm with initial average particle radius $\langle r_o \rangle = 7.05$ μm inside the experimental region 120 μm × 150 μm. The next model shown in Fig. 4b was obtained during the packing process PP0 (the minimal thickness of the liquid layer was $\ell = 0.1$ μm, and the experimental region 120 μm × 100 μm). The initial surface area fraction of the solid phase after the packing process is rather difficult to estimate and is lower than expected (66%) because of the wall effect during packing. Therefore, the narrower experimental region (dashed box on Fig. 4b) in which the surface area fraction of solid is 75% will be considered. Because the solution-precipitation model and contour coarsening model make no assumption about the starting model system, the packed system obtained by PP0 (Fig. 4b) has been used as the starting model system.

TABLE I Values used in computer simulation of grain boundary migration during liquid phase sintering of an Al_2O_3–glass System

Variable	Description	Values	Reference
C_o	Equilibrium concentration of liquid	29.00 mol%	15
D_L	Diffusivity of the solid in the liquid	1×10^{-10} m^2/s	16
Ω	Molecular volume of the solid	4.25×10^{-29} m^3 (Al_2O_3)	—
γ_{sl}	Solid/liquid interfacial energy	0.5 J/m^2	17
T	Sintering temperature	1873 K	—

For the Al_2O_3–magnesium aluminosilicate glass system with an equilibrium composition of liquid 14.6 MgO, 44.1 Al_2O_3, and 41.3 SiO_2, in wt % [14], the data given in Table I were used. On the basis of the time exponent and activation energy obtained in their experiments, Hamano and Miura [18] and Kalita [19] proposed that densification of an alumina–glass system is controlled by diffusion during solution-precipitation. Kwon and Messing [14] have analyzed densification of this system also. Their analysis and observations consistently supported interface reaction-controlled densification during solution-precipitation. In the present simulation the latter results—that the coarsening will be controlled by the interface reaction—were used. All calculations were performed on 256×256 mesh points. The larger mesh would improve the accuracy of the computation, but this change requires a super computing platform because increasing the mesh size (i.e., decreasing the unit length of the mesh) increases the calculation time tremendously.

In this section, a selection of computed results is presented to illustrate the application of the defined simulation models for the solution-precipitation processes and the contour coarsening process. The initial concentration of liquid phase was as shown in Fig. 5. The flat surfaces in Fig. 5c represent the solid phase where the boundary concentrations (8) were extended across the entire domains because the contours were initially circular. However, for the computation of the evolution of microstructure only the boundary points' concentration $C(\mathbf{r}_j^s)$ is of interest.

After a few minutes, solution-diffusion-precipitation processes are just beginning to occur along the solid/liquid boundary interfaces. The driving force of those processes is not the difference in the contour size, but the concentration gradient between solid and liquid phases. Smaller contours have the highest concentration levels, and they dissolve in the liquid matrix. The fine contours will disappear at the start of coarsening, resulting in an increase in mean size. Dissolved atoms diffuse through the liquid layer or through the liquid matrix, and precipitate on the larger contours. During this stage, the liquid thickness remains nearly constant because dissolution and precipitation simultaneously take place over short distances. The smaller dissolving contours give way to new packing of small and large contours. The smaller contours tend to be preferentially located near the large contours, as suggested in Ref. [20], because the large contours always grow, resulting in the surrounding contours being small. Further morphological changes may occur by large contours growing during contour coarsening.

Fig. 6a and 6b show the shape and location of the center of the model system contours. From simulation results at various times 20 and 40 min, it can be seen that morphological evolution and migration depend on the contour's location. In the present simulation, the small contours tend to be located near the large contours during PP1 packing process. The large contours with small contours as neighbors have extensive grain boundary movement because they have the fastest growth (e.g., contours numbered with **1** and **2** with corresponding dashed regions shown in Fig. 6). This means that small contours, which are very close to bigger ones, dissolve very quickly and will disappear. The growth of larger contours (the precipitated areas) does not occur uniformly around the contours. The largest shape distortion in center-to-center direction is a result of intercontour diffusion interactions at relatively small intercontour distances (large concentration gradient). It can be seen also that a diffusion field surrounding some contours has no influence on the precipitation process because of relatively large distances between contours. Such contours dissolve very slowly. These changes in the microstructure are more visible on Fig. 6b. After 80 min (Fig. 7), most of the smallest contours have disappeared, some of the smaller contours are still dissolving, and the bigger ones are growing only. Evident is the decrease in the number of contours and an increase in the average contour's size with simulation time. By such model system evolution, it can be concluded that although the liquid layer thickness slowly increases with time, which will certainly alter the flux of dissolving material, the average liquid thickness remains approximately constant as a result of a moving grain boundary. All of these processes will be ended by completely reaching a uniform concentration distribution.

Figure 8a shows the dependence of normalized (by the initial average contour radius $\langle r_o \rangle$) contour radius on simulation time, where time dependent contour radii were calculated through

$$r_s(t) = \frac{1}{n_s} \sum_{i=1}^{n_s} r_i^s(t) \quad (s = 1, 2, \ldots, N)$$

as an approximation. Similar dependence can be obtained applying expression (7) for time dependent contour area $A^s(t)$ in 2-D section (Fig. 8b), where $\langle A_o \rangle$ is the initial average contour area. It can be seen that only the largest contours grow, the small contours dissolve and disappear, and contours with radii close to the average (approximately) do not change size. Further, as a result of the solution-precipitation process, and the subsequent contour coarsening process, some of the

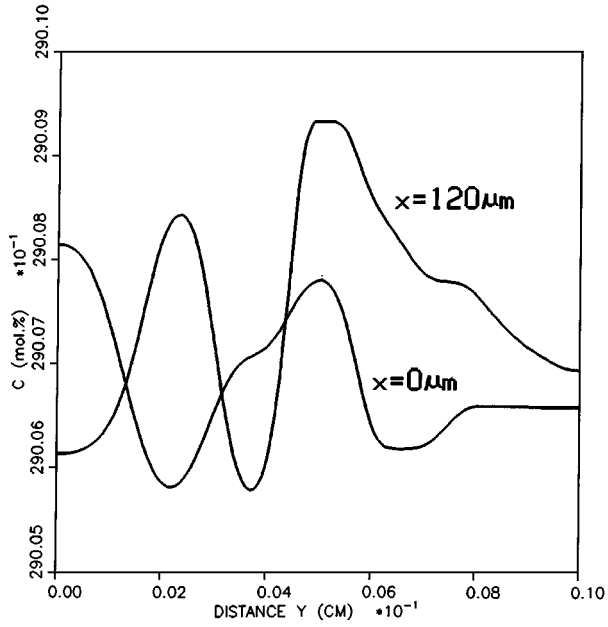

(a)

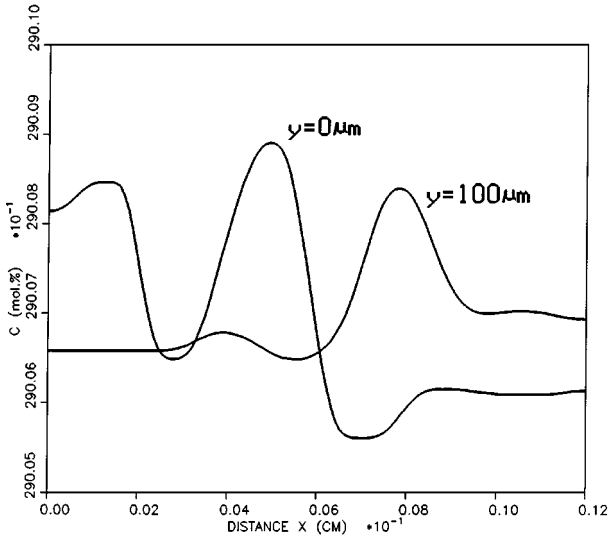

(b)

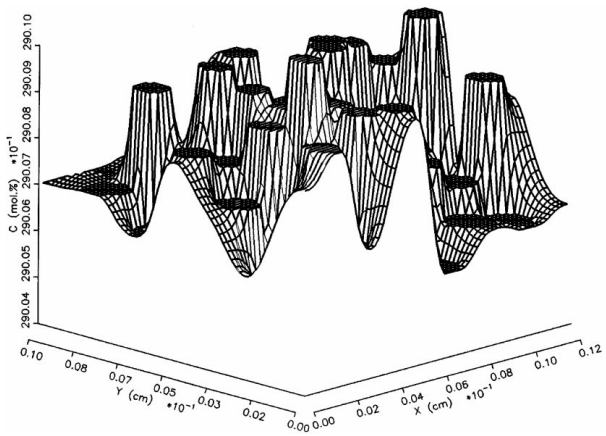

(c)

Figure 5 Initial concentration profile of liquid phase: (a) initial boundary concentration of liquid along *y*-axis, (b) initial boundary concentration of liquid along *x*-axis, (c) 3-D initial concentration of liquid and solid (the flat surfaces represent the solid phase). For this figure only, the mesh size was 65 × 65.

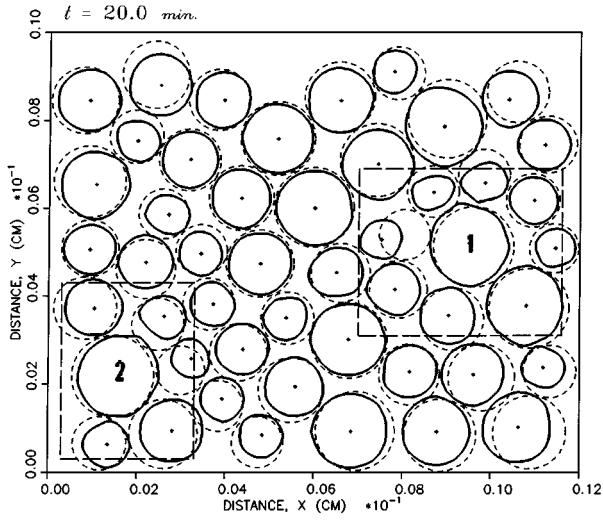

(a)

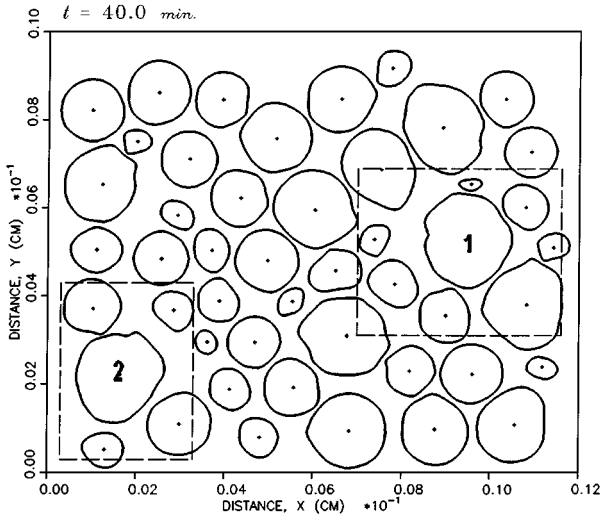

(b)

Figure 6 Simulation results of microstructural changes (dashed circular lines denote starting model geometry): (a) after 20 min, (b) after 40 min.

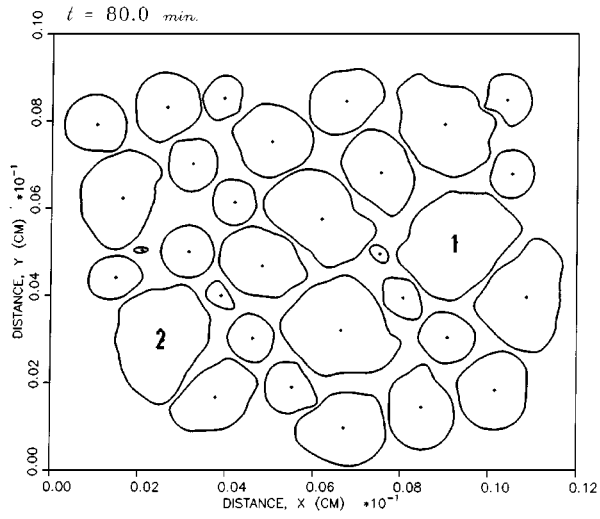

Figure 7 Simulation results of microstructural changes after 80 min.

contours with initial radius close to the average radius show a tendency toward dissolution and precipitation at the same time: such contours grow on one side and dissolve on the other. Fig. 9a shows normalized contour

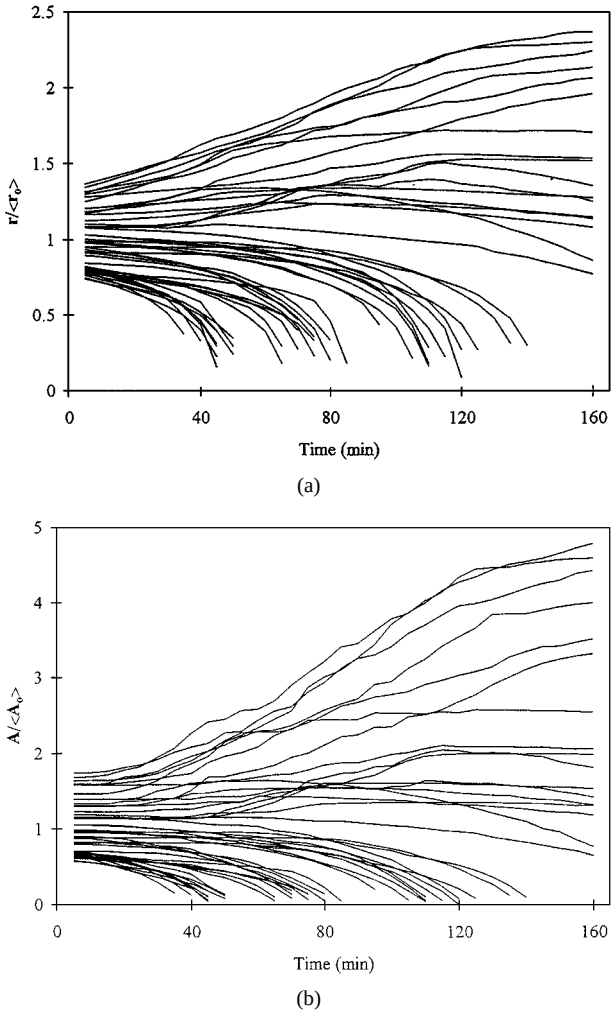

Figure 8 Contour size vs. simulation time: (a) the normalized (by the initial average contour radius) contour' radius vs. simulation time, (b) the normalized (by the initial average contour area) contour area verses simulation time.

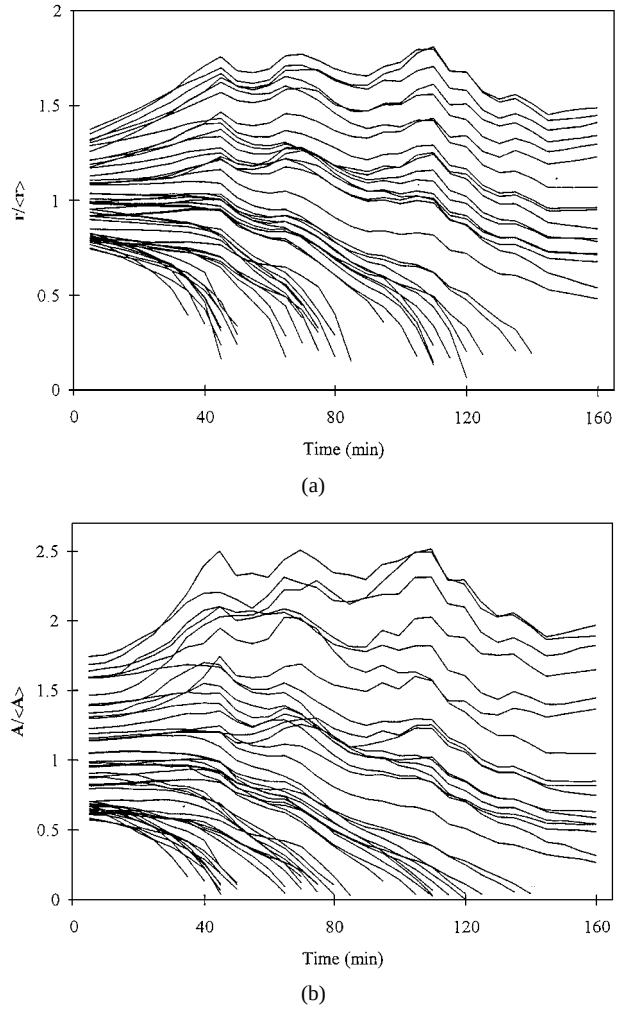

Figure 9 Contour size vs. simulation time: (a) the normalized (by the time-dependent average contour radius) contour' radius vs. simulation time, (b) the normalized (by the time-dependent average contour area) contour area verses simulation time.

radius as a function of time, where the average radius $\langle r \rangle$ is also a function of time, i.e.,

$$\langle r(t) \rangle = \frac{1}{N} \sum_{s=1}^{N} r_s(t)$$

Fig. 9b shows normalized contour area as a function of time, where the average contour area $\langle A \rangle$ is also a function of time, i.e.,

$$\langle A(t) \rangle = \frac{1}{N} \sum_{s=1}^{N} A^s(t)$$

The contours with radius smaller than average one have the negative slope curve and opposite. It can be seen that the latter ones, and for sufficiently long simulation time the larger contours, have the slopes curve approximately equal zero (i.e., these contours grow at the same rate as the average). A similar result was obtained by Voorhees and Glicksman [21].

A general conclusion can be drawn that the largest contours grow at the expense of the surrounding smaller contours. Because of this conclusion, the distances between the interfaces of the large contours that are located near one another decrease with simulation time. However, when small contours have disappeared, some large contours can grow at the expense of the others. This process probably depends on the size difference between these large contours. As Akaiwa and Voorhees have concluded [22], this process must be fairly rare, for it depends on two large contours of nearly the same size being located near each other.

It can be seen also that during coarsening, the sizes of contours and their centers' locations change with simulation time. The global (x_c, y_c) dependence shows that most of the contours have a rigid body motion. The migration of the contours is a result of the nonuniform concentration gradient over their surfaces. For some contours this migration can be significant inside the experimental region. Even small changes in the locations of the contours relative to one another can have large effects on the resultant morphological evolution of model system. The analysis of the contour center locations in both x and y directions versus sintering time is shown in Figs 10 and 11.

Fig. 10 shows the center position normalized by the initial average contour radius $\langle r_o \rangle$ as a function of

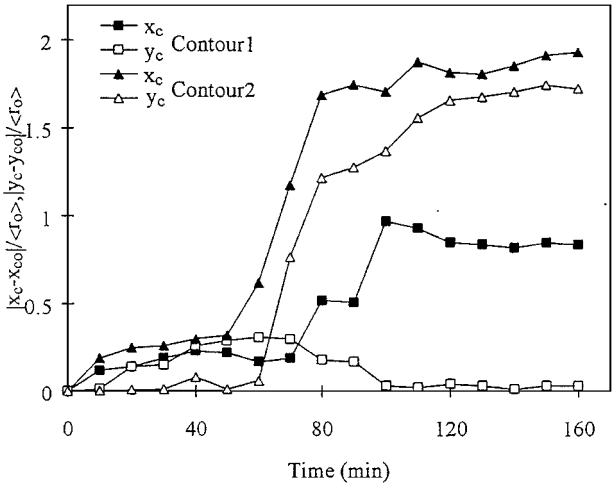

Figure 10 The center positions of the contour as a function of simulation time using (x_{co}^1, y_{co}^1) and (x_{co}^2, y_{co}^2) as the initial center positions for the contour **1** and contour **2** respectively.

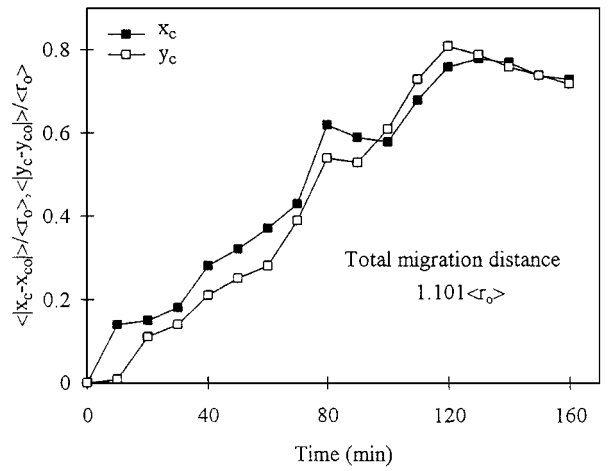

Figure 11 The average center position of the contour as a function of simulation time using $(\mathbf{x}_{co}, \mathbf{y}_{co})$ as the initial center position vectors.

simulation time. The positions (x_{co}^1, y_{co}^1) and (x_{co}^2, y_{co}^2) are chosen as the initial center positions for the contour **1** and contour **2**, respectively. As it can be seen from Figs 6 and 7, both contours grow with time. At the beginning, the smaller contours that are very close to the contour **2** dissolve very quickly; therefore, starting migration of this contour is significant and larger than the migration of the contour **1**. For the larger simulation time, the migration distances for the two contours depend on surrounding contours and the corresponding nonuniform concentration gradient. A similar conclusion can be drawn for the average time-dependent center positions for all contours of the model system (Fig. 11). The total migration distance for the model system is $1.101 \cdot \langle r_o \rangle$, or approximately the initial radius of the contour.

From the examination of microstructural changes (Fig. 6), it can be concluded that the contours principally assume a rounded shape because the amount of liquid is fairly large. However, in a late stage of liquid phase sintering, it can be assumed (Fig. 7) that some of

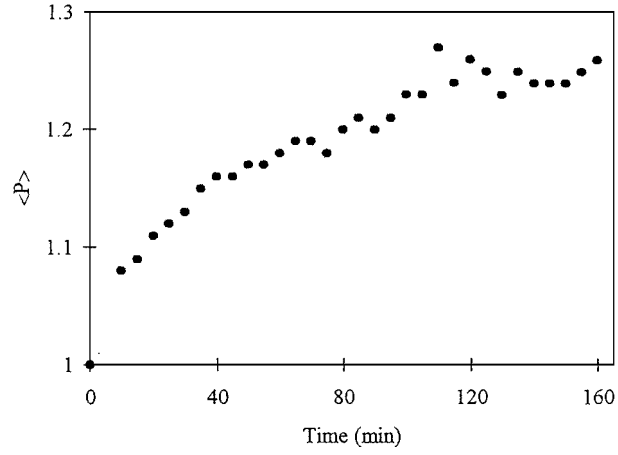

Figure 12 The dependence of the average shape factor on the simulation time.

the contour contacts can be approximately flattened, as it has been observed in Ref. [14]. Because the present simulation is performed without the shape restriction, no overlapping contours were found.

If L^s is the length of the interface on s-th contour, then the shape factor can be defined by

$$P^s \equiv \frac{L^s}{2\pi r_s} = \begin{cases} 1 & \text{for a circular contour} \\ >1 & \text{for a noncircular contour} \end{cases}$$

This factor can be used for estimation of the degree of noncircularity of the model system contours. The average shape factor versus simulation time for our model experiment is shown in Fig. 12. The starting value of $\langle P \rangle$ is 1 because all contours are initially circular. It can be seen that this factor is time-dependent with the tendency to approach a constant value for a longer simulation time. Akaiwa and Meiron [23] studied the late stage of nucleation and Ostwald ripening in two dimensions using a boundary integral formulation. Although the numerical model in the present simulation is quite different from their analytical and numerical models, time-dependent shape factor function and model system contour configuration are very similar.

The dominant process through solution-precipitation and grain coarsening is grain growth. The numerical model for the grain growth similar to the model [24] can be used to predict how the grain size of a microstructure develops during sintering. The results of grain growth versus sintering time for the two large contours **1** and **2** are plotted on Fig. 13. The discrete values of growth were computed as average radius growth values for all boundary points of contour. It can be seen that both contours have the similar growth, which rapidly increases with time. For a longer simulation time, the contour **1** almost has no small contours as neighbors, thus the growth rate slowly approaches its limiting value. For contour **2**, there are a few small contours as neighbors, thus its growth rate slowly increases. The average growth for "growing contours" of the model system is also plotted on Fig. 13. By comparing these three curves, it can be concluded that "growing contours" grow similarly to contour **1**, with the tendency to

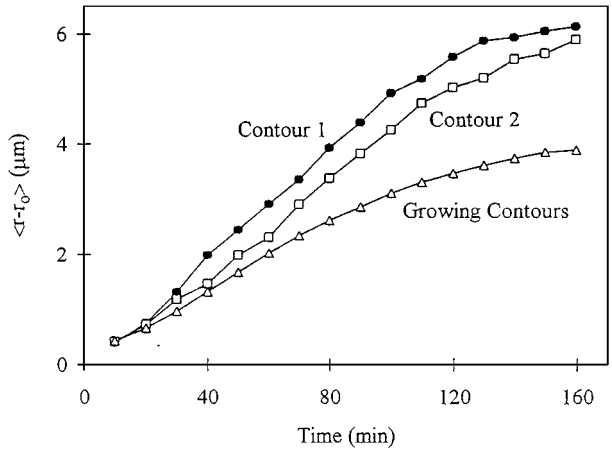

Figure 13 Simulated average radius growth vs. simulation time for contours **1** and **2**, and for "growing contours."

approach a constant value as time increases. Its lower average growth is a result of the fact that a diffusion field surrounding some contours has not the same influence on the solution-precipitation process because of different distances between contours. Fig. 14 shows the average growth for all contours. For a short simulation time, small contours dissolve very quickly, and larger contours grow relatively slowly. Therefore, dissolution effect is greater than precipitation effect. During sintering, most of small contours will disappear resulting in an increase in average contour radius (i.e. average contour area). It is clear that after long sintering time, the growth should decrease because of a decreasing amount of solid phase and increasing intercontour distances.

Future modification of the simulation model should include a more realistic packing process by taking into account the fairly small amount of liquid phase, and that the particles are surrounded by small and large pores. For such a rigorous simulation model, some of the required information already exists, but clearly full constitutive description must await further studies of liquid phase sintering.

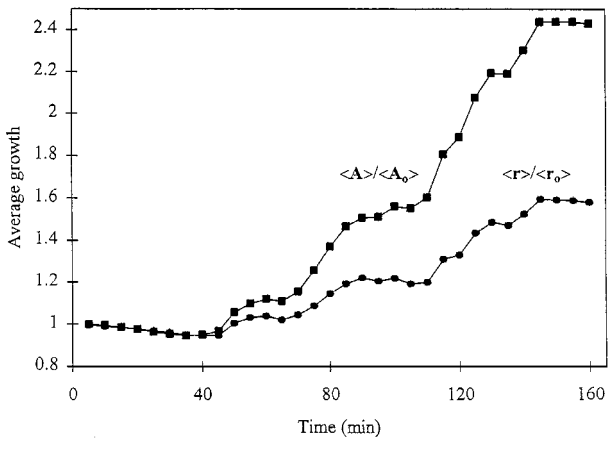

Figure 14 Average radius (area) growth verses simulation time for "all contours."

5. Conclusions

This paper outlines a computer-based method for simulation of grain boundary migration on liquid/solid interfaces during liquid phase sintering. The theoretical basis of such analysis is general and applicable to any multicomponent ceramic system. The simulation method developed is based on the defined submodels for initial model system definition, solution-precipitation process, and grain coarsening process. With the initial model system based on randomly distributed particles, the packing processes PP0 and PP1 were simulated by a settling procedure in which contours are settled on the bottom of the experimental region, simulating gravity, and toward the center of experimental region, respectively. The solution-precipitation and grain coarsening were modeled based on the corresponding model system, which restructures itself so that larger particles can grow by transfer of dissolved atoms through the liquid phase. Such a simulation method can be used to assist in analysis of experimental data and in the optimization of sintering in the presence of a liquid phase.

Acknowledgements

The author would like to acknowledge helpful discussions with Academician M. M. Ristic, Serbian Academy of Sciences and Arts, Yugoslavia, and Professors R. M. Spriggs and V. R. W. Amarakoon, Alfred University, USA. The present work was performed under the project "Prognosis of Materials Properties" supported financially by the Ministry for Science and Technology of Republic Serbia, Yugoslavia.

References

1. F. V. LENEL, Trans. *AIME* **175** (1948) 878.
2. Z. S. NIKOLIC, R. M. SPRIGGS, V. R. W. AMARAKOON and M. M. RISTIC, in 98th Annual Meeting of the American Ceramic Society, Indianapolis, IN, April 15, 1996 (Computational Modeling of Materials and Processing Symposium, Paper No. SX-6-96).
3. Z. S. NIKOLIC, *Sci. of Sintering*, **28** Special Issue (1996) 55.
4. Z. S. NIKOLIC and R. M. SPRIGGS, *Sci. of Sintering* **26** (1994) 1.
5. Z. S. NIKOLIC, R. M. SPRIGGS and M. M. RISTIC, *Z. Metallkd.* **83** (1992) 769.
6. H. FISCHMEISTER and G. GRIMVALL, in "Sintering and Related Phenomena," edited by G. C. Kuczynski (Plenum Press, New York, 1973) p. 119.
7. J. CRANK, "The Mathematics of Diffusion" (Oxford University Press, Oxford 1956).
8. B. R. DEWEY, "Computer Graphics for Engineers" (Harper & Row Publishers, New York, 1988).
9. T. O. SAETRE and N. RYUM, *J. Sci. Comp.*, in Proc. of Fall TMS meeting (1992).
10. A. C. F. COCKS and S. P. GILL, *Acta Mater.* **44** 12 (1996) 4765.
11. S. C. HANSEN and D. S. PHILLIPS, *Philos. Mag. A* **47** (1983) 209.
12. M. P. HARMER, in "Structure and Properties of MgO and Al_2O_3 Ceramics," edited by W. D. Kingery (Am. Ceram. Soc., Columbus, Ohio, 1984) p. 679.
13. Y. K. SIMPSON, C. B. CARTER, K. J. MORRISEY, P. AUGELINI and J. BENTLEY, *J. Mater. Sci.* **21** (1986) 2689.
14. OH-HUN KWON and G. L. MESSING, *J. Am. Ceram. Soc.* **73** (1990) 275.

15. E. M. LEVIN, C. R. ROBBINS, and H. F. MCMURDIE in "Phase Diagrams for Ceramics," 2nd edition (Am. Ceram. Soc., Columbus, Ohio, 1981) p. 246.
16. Y. OISHI, R. TERAI, and H. UEDA, in "Materials Science Research," Vol. 9, Mass Transport Process in Ceramics, edited by A. H. Heuer (Plenum Press, New York, 1985) p. 297.
17. OH-HUN KWON and G. L. MESSING, *Acta Metall.* **39** (1991) 2059.
18. K. HAMANO and K. MIURA, in "Report Research Laboratory of Engineering Materials," No. 2 (Nagoya University, Nagoya, Japan 1977) p. 77.
19. G. E. KALITA, *Refractories* (Engl. Transl.), **20** (1979) 53.
20. M. MARDER, *Phys. Rev. Lett.* **55** (1985) 2953.
21. P. W. VOORHEES and M. E. GLICKSMAN, *Met. Trans.* **15A** (1984) 1081.
22. N. AKAIWA and P. W. VOORHEES, *Phys. Rev.* **49** (1994) 3860.
23. N. AKAIWA and D. I. MEIRON, *ibid.* **54**, R13 (1996).
24. Z. S. NIKOLIC, R. M. SPRIGGS and M. M. RISTIC, *Sci. of Sintering* **24** (1992) 49.

Received 1 November 1997
and accepted 16 July 1998